

Article

# Structural and Spectroscopic Characterization of Co(II) Bis(Benzenedichlorodithiolate): An Intermediate in Hydrogen Evolution Catalysis

Virginia A. Larson , Jeff W. Kampf and Nicolai Lehnert \* 

Department of Chemistry and Department of Biophysics, University of Michigan, Ann Arbor, MI 48109-1055, USA; vlarson@umich.edu (V.A.L.)

\* Correspondence: lehnertn@umich.edu

**Abstract:** Co bis(benzenedithiolate) type complexes have captivated chemists for decades for their interesting geometric and electronic structures and more recently, for their impressive ability to mediate the hydrogen evolution reaction (HER) both photo- and electrocatalytically. However, these complexes have nearly exclusively been characterized in their air-stable Co(III) oxidation states. In this work, Co(II) bis(benzenedichlorodithiolate) was prepared by chemical and electrochemical one-electron reduction. This reduced Co(II) complex was characterized by X-ray crystallography and in-depth spectroscopic studies—including UV-Vis, magnetic circular dichroism, and electron paramagnetic resonance spectroscopy.  $[\text{Co}(\text{II})(\text{Cl}_2\text{bdt})_2]^{2-}$  is thereby shown to be a square planar complex, with a primarily metal-centered reduction, and an  $S_t = 1/2$  spin state. This study informs our understanding of the first step in the HER catalytic cycle of Co bis(benzenedithiolate) type complexes and paves the way for future mechanistic studies on this catalyst family.

**Keywords:** Co bis(benzenedithiolate) complexes; hydrogen evolution reaction; reaction intermediates; energy; electrocatalysis



**Citation:** Larson, V.A.; Kampf, J.W.; Lehnert, N. Structural and Spectroscopic Characterization of Co(II) Bis(Benzenedichlorodithiolate): An Intermediate in Hydrogen Evolution Catalysis. *Inorganics* **2024**, *12*, 75. <https://doi.org/10.3390/inorganics12030075>

Academic Editors: Axel Klein, S. Masoud Nabavizadeh and Fatemeh Niroomand Hosseini

Received: 7 February 2024  
Revised: 25 February 2024  
Accepted: 26 February 2024  
Published: 29 February 2024



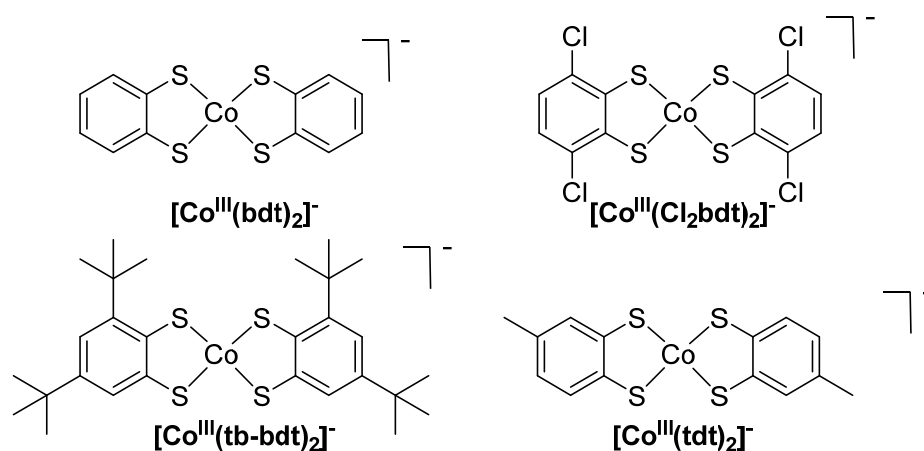
**Copyright:** © 2024 by the authors. Licensee MDPI, Basel, Switzerland. This article is an open access article distributed under the terms and conditions of the Creative Commons Attribution (CC BY) license (<https://creativecommons.org/licenses/by/4.0/>).

## 1. Introduction

Understanding the mechanisms that catalysts use to conduct their reactions allows for the optimization and troubleshooting of catalytic processes. Previously, others and ourselves have shown that Co bis(benzenedithiolate) type complexes are highly active catalysts for the Hydrogen Evolution Reaction (HER). This includes homogenous electrocatalytic HER [1], homogeneous photocatalytic HER [1,2], and heterogeneous HER when either physisorbed to electrode surfaces [3–5], as active sites in MOFs [6–9], or, as recently reported, when covalently attached to an electrode surface [10]. These catalysts perform well in HER compared to other heterogenized earth-abundant transition-metal molecular complexes that have been reported in the literature [10–12]. However, Co bis(benzenedithiolate) type complexes are often shown to decline in activity over time [4,5,10]. Therefore, it is desirable to better understand the molecular mechanism of these catalysts to elucidate the reason(s) for catalyst failure and to obtain insight into how these catalysts function in HER, both homogeneously and heterogeneously.

As Co bis(benzenedithiolate) type complexes have been studied for roughly 60 years, there is much known about their geometric and electronic structure. Initial studies by Gray, Billig, and others in the 1960s focused on their interesting electronic properties, with the benzenedithiolate being a potential non-innocent ligand [13–15]. These complexes, in their  $\text{Co}^{\text{III}}$  forms, are square planar and monomeric, though some derivatives not discussed here-in may dimerize [2,14]. The complexes discussed in this paper are shown in Scheme 1. The benzenedithiolate ligand has further been shown to be non-innocent and partially oxidized in the ground state. The ground state is best described as a mix of 50–70%  $\text{Co}^{\text{III}}(\text{L})_2$

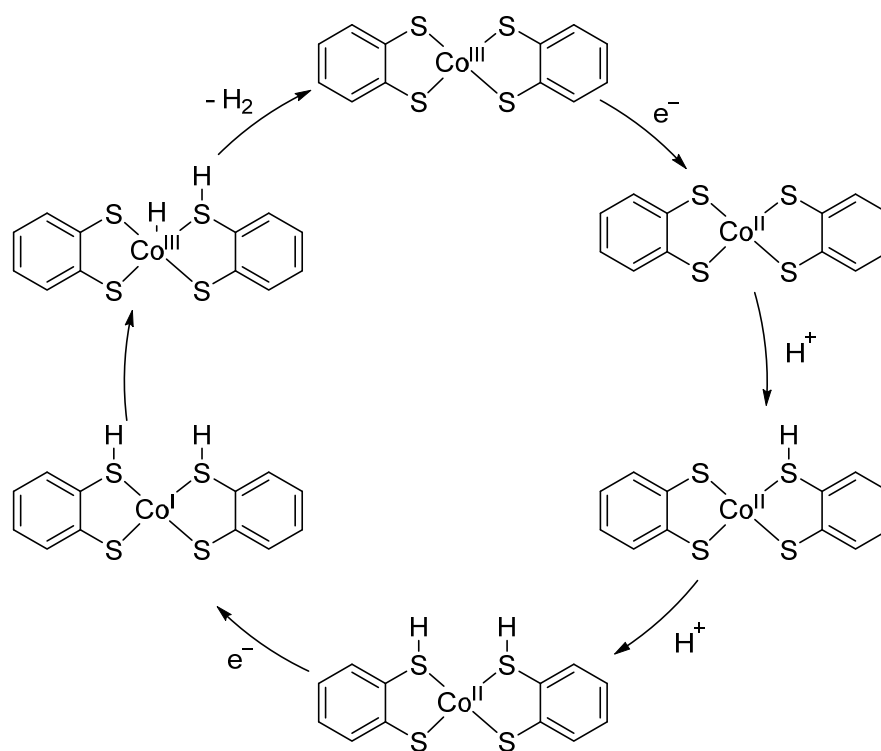
and 50–30%  $\text{Co}^{\text{II}}(\text{L}^{\bullet})(\text{L})$  character [16,17], due to the  $\text{Co}(\text{d})$  and dithiolate( $\pi$ ) orbitals being closely matched in energy and participating in strong covalent bonding.



**Scheme 1.** Structures of complexes discussed in this paper. Ligand abbreviations are as follows, bdt = benzene-1,2-dithiolate,  $\text{Cl}_2\text{bdt}$  = 3,6-dichlorobenzene-1,2-dithiolate,  $\text{tb-bdt}$  = 3,5-di-tert-butylbenzene-1,2-dithiolate, and  $\text{tdt}$  = toluene-3,4-dithiolate.

As catalysts for HER [1–5,10], some information has been obtained about the putative HER mechanism of these complexes. However, how the non-innocent benzenedithiolate ligands impact HER catalysis exactly is not well understood. There are nominally four steps to HER: two electron transfers ( $E'$  steps) and two proton transfers ( $C'$  steps). Cyclic voltammetry shows that the first step of the HER reaction by Co bis(benzenedithiolate) type complexes is reduction from the  $\text{Co}^{\text{III}}$  to the  $\text{Co}^{\text{II}}$  state, with catalytic activity setting in at or after the  $\text{Co}(\text{III}/\text{II})$  couple. The second step is protonation, as the  $\text{Co}(\text{II}/\text{I})$  couple is not observed at any accessible potential in the absence of acid. The order of the next two steps has been suggested by density functional theory (DFT) calculations [18] but has not been determined experimentally. Specifically, Hans and Eisenberg suggested an ECCE mechanism, where protonation initially occurs on the sulfur atoms of the benzenedithiolate ligands, and after the second reduction, the  $\text{Co}^{\text{I}}$  center is protonated to generate a hydride, and then the resulting  $\text{Co}(\text{III})\text{-H}$  and remaining  $\text{H-S}_{\text{bdt}}$  proton form hydrogen intramolecularly. This mechanism is illustrated in Scheme 2.

Our group is interested in studying the HER activity of these  $[\text{Co}(\text{bdt})_2]^-$  type complexes when immobilized onto electrode surfaces (bdt = benzene-1,2-dithiolate; see Scheme 1). In particular, we have studied the complexes when physisorbed to graphitic surfaces [3,4]. In this case, the geometries of the intermediates featured in the mechanism are particularly important: it is possible that during the catalytic cycle, if the catalyst distorts from its square-planar structure, its ability to  $\pi$ -stack with the graphitic electrode is disrupted, promoting dissociation of the physisorbed catalyst from the electrode surface. Specifically, the geometric structure of the  $\text{Co}(\text{II})$  form is unknown. Solis and Hammes-Schiffer calculated that in the quartet state, the  $\text{Co}(\text{II})$  form would be tetrahedral, while the doublet state of  $\text{Co}(\text{II})$  would lead to a square-planar geometry [18]. If the  $\text{Co}(\text{II})$  form is indeed in the quartet state and tetrahedral, this would promote dissociation of the complex from the graphitic surface. In their calculations, the tetrahedral quartet structure is indeed slightly energetically favored [18]. In this paper, however, we show that the  $\text{Co}(\text{II})$  form of the complex is in fact in the doublet spin state with a square-planar geometric structure, providing further experimental insight into the HER mechanism of Co bis(benzenedithiolate) type complexes.



**Scheme 2.** Proposed mechanism by Solis and Hammes-Schiffer [18]. This mechanism was calculated to be preferred by  $[\text{Co}(\text{bdt})_2]^-$ ,  $[\text{Co}(\text{Cl}_2\text{bdt})_2]^-$ , and  $[\text{Co}(\text{tdt})_2]^-$ . Here, the parent  $[\text{Co}(\text{bdt})_2]^-$  complex is used for illustration. See Scheme 1 for structures of the other species.

Interestingly, a computational study on the similar Co bis(diaryldithiolene) type complexes, which are also known to be active for HER [19,20], reported the dianion to have a square-planar geometry with a  $S_t = 1/2$  ground state [19]. Specifically, the doublet square-planar species was predicted to have the highest occupied molecular orbital (HOMO) with primarily Co character. In contrast, the higher energy tetrahedral quartet complex was calculated to have more sulfur character in its HOMO. The ground state and geometry predicted for the Co bis(diaryldithiolene) complex were then thought to promote protonation of the Co center instead of at a sulfur atom in the HER mechanism [19,21].

While there have been extensive studies on  $[\text{Co}(\text{bdt})_2]^-$  type complexes and their electronic structure [14], much less experimental work is available for the reduced Co(II) form, which is likely due to the fact that these species are very air sensitive. When the early research on these complexes was being performed, the preparation of pure samples was challenging [22]. Some research was conducted on  $[\text{Co}(\text{tdt})_2]^{2-}$  and  $[\text{Co}(\text{tb-bdt})_2]^{2-}$  (tdt = toluene-3,4-dithiolate and tb-bdt = 3,5-di-tert-butylbenzene-1,2-dithiolate). In a study by Sawyer et al., reported in 1986, the  $[\text{Co}(\text{tdt})_2]^-$  complex was electrochemically reduced in MeCN, perhaps incompletely, as the 660 nm peak persisted, to obtain a UV-Vis spectrum of the Co(II) form [22]. The reduced  $[\text{Co}(\text{tb-bdt})_2]^{2-}$  form was also prepared by electrochemical reduction at reduced temperatures ( $-25^\circ\text{C}$ ), and the UV-Vis spectrum was published in a thesis in 2005 [23]. A 2012 study which reported a variety of  $\text{M}(\text{bdt})_2$  type complexes included the synthesis and characterization of  $(\text{Ph}_4\text{P})_2\text{Co}(\text{II})(4\text{-cyanobenzene-1,2-dithiolate})_2$  [24]. This species was characterized by X-ray crystallography, magnetic susceptibility, and powder electron paramagnetic resonance (EPR) spectroscopy at 77 K, showing that it is a square-planar  $S_t = 1/2$  species. However, this Co complex has not been reported for HER catalysis and lacks further spectroscopic studies, such as UV-Vis and magnetic circular dichroism (MCD) spectroscopy. Nevertheless, these data are consistent with our observations, see below. Additionally, there have been a few studies on Co(II) dithiolene complexes with non-bdt type ligands [19,22].

Further, none of the intermediates following Co(II) formation in the proposed HER mechanism illustrated in Scheme 2 have been experimentally isolated or studied. The  $[\text{Co}(\text{bdt})_2]^-$  type complexes are adept at electrocatalytic HER, and these intermediates can be expected to be short-lived under catalytic conditions, which makes their isolation challenging.

In this study, we set out to investigate the reduced Co(II) intermediates to further determine the HER mechanism of Co bis(benzenedithiolate) type complexes and possibly identify points of failure of these catalysts, specifically if the one-electron reduced Co(II) form is tetrahedral and therefore promotes catalyst dissociation from the electrode surface. For this study, we used  $[\text{Co}(\text{Cl}_2\text{bdt})_2]^-$ , as it is a highly active catalyst and the required ligand is commercially available ( $\text{Cl}_2\text{bdt}$  = 3,6-dichlorobenzene-1,2-dithiolate). Herein, we show that the Co(III) complex can be reduced by chemical or electrochemical means to the Co(II) oxidation state. X-ray crystallography shows that the Co(II) complex retains the same square-planar geometry as the starting Co(III) complex. This result shows that reduction alone does not promote catalyst dissociation from the electrode surface by twisting the structure to tetrahedral. We further report a detailed spectroscopic characterization of this Co(II) species by MCD, EPR, and UV-Vis spectroscopy.

## 2. Results and Discussion

### *Synthesis and Characterization of $[\text{Co}^{\text{II}}(\text{Cl}_2\text{bdt})_2]^{2-}$*

The complex  $[\text{TBA}][\text{Co}^{\text{III}}(\text{Cl}_2\text{bdt})_2]$  (TBA = tetrabutylammonium cation) was synthesized according to literature procedures [5,15]. The reduced complex  $[\text{Co}^{\text{II}}(\text{Cl}_2\text{bdt})_2]^{2-}$  can be prepared chemically, by the addition of a stoichiometric reducing agent, cobaltocene, or electrochemically, by controlled potential reductive electrolysis. As expected, given the reported UV-Vis spectra for  $[\text{Co}^{\text{II}}(\text{tdt})_2]^{2-}$  and  $[\text{Co}^{\text{II}}(\text{tb-bdt})_2]^{2-}$  [22,23], the Co(II) form gives a light yellow solution, in contrast to the dark blue color of the Co(III) species. The comparison of the UV-Vis spectra is shown in Figure 1. The Co(II) form is highly air sensitive and quickly oxidizes in air to return to the starting Co(III) form, as shown in Figure S1.

$[\text{Co}^{\text{II}}(\text{Cl}_2\text{bdt})_2]^{2-}$  can also be prepared by electrochemical reduction of  $[\text{Co}^{\text{III}}(\text{Cl}_2\text{bdt})_2]^-$ . This approach is expected to form high-concentration solutions of  $[\text{Co}^{\text{II}}(\text{Cl}_2\text{bdt})_2]^{2-}$ , as the Co(III/II) couple of the complex is well behaved, and this method has been used previously to prepare reduced  $\text{Co}(\text{bdt})_2$  type species [22,23]. Indeed, the Co(III) complex is cleanly converted to Co(II) upon applying a reducing potential in 0.1 M  $[\text{TBA}](\text{PF}_6)$  in acetonitrile under Ar, as shown in Figure S2. This formation of the Co(II) complex was confirmed by UV-Vis spectroscopy, see Figure S3. The resulting, reduced complex is the same as the one obtained by chemical reduction with cobaltocene. However, for the remaining studies reported here, chemical reduction was used to prepare the Co(II) complex.

High-quality crystals of the Co(II) species were obtained by slow solvent evaporation of the chemically reduced species in butyronitrile at low temperatures. X-ray crystallography of this species shows two cobaltocenium cations per each square-planar  $[\text{Co}^{\text{II}}(\text{Cl}_2\text{bdt})_2]^{2-}$  dianion. The dianion is strictly planar with the sum of the S-Co-S angles summing to  $360.0^\circ$ , as shown in Figure 2. Another way to evaluate the geometry of a four-coordinate complex is with the  $\tau_4$  parameter, where  $\tau_4 = 0.00$  for ideal square-planar geometry and  $\tau_4 = 1.00$  for ideal tetrahedral geometry [25]. The  $[\text{Co}^{\text{II}}(\text{Cl}_2\text{bdt})_2]^{2-}$  complex reported herein is calculated to have a  $\tau_4 = 0.02$ , which further confirms its square-planar geometry. Comparison to the crystal structure of the Co(III) species, reported by McNamara et al. [2] shows that this is a primarily metal-based reduction, as the aryl ligand bond distances show very little change (see Table 1). This suggests that while Solis and Hammes-Schiffer predicted that the tetrahedral quartet state of Co(II) would be favored [18], under these conditions, the complex is experimentally found to be square-planar. This suggests that the species is instead a doublet Co(II) complex.

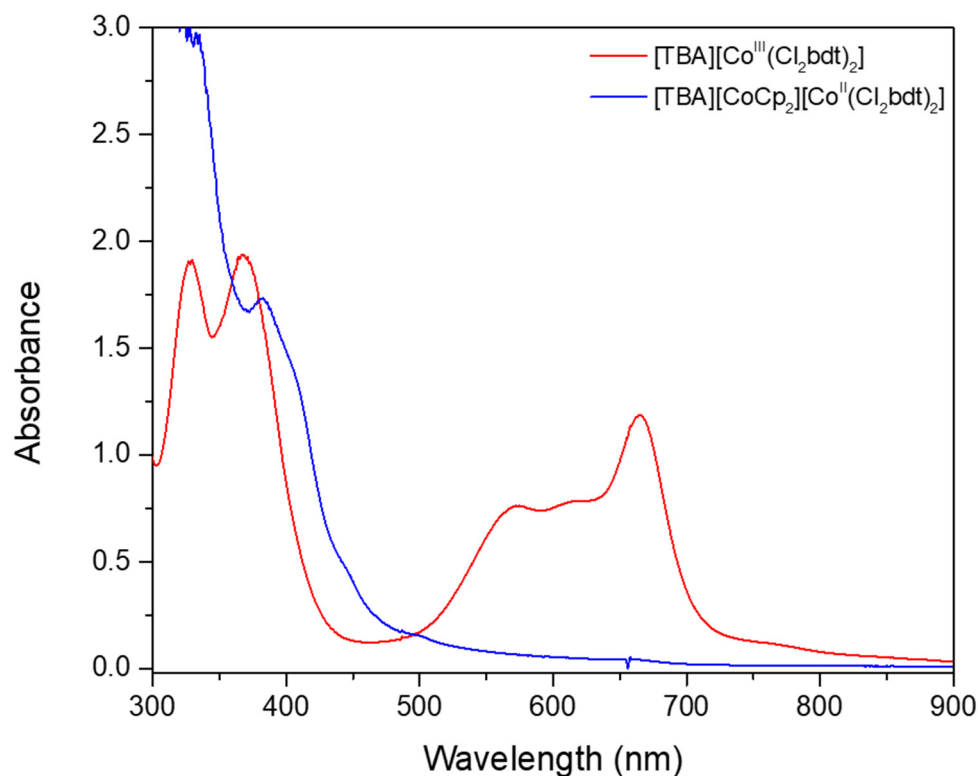


**Figure 1.** Comparison of the UV-Vis spectra of the complexes  $[\text{Co}^{\text{III}}(\text{Cl}_2\text{bdt})_2]^-$  and  $[\text{Co}^{\text{II}}(\text{Cl}_2\text{bdt})_2]^{2-}$ , each at 0.1 mM in THF at room temperature (RT). The data for the Co(II) species were taken under an inert atmosphere, while those for the Co(III) complex were obtained in ambient air.

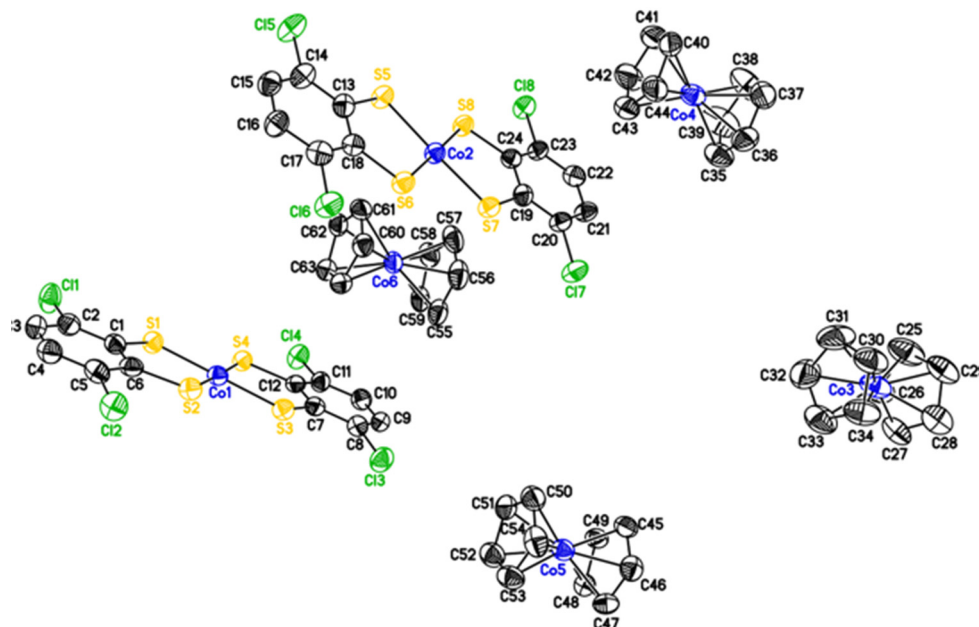


**Figure 2.** X-ray crystal structure of  $[\text{CoCp}_2]_2[\text{Co}^{\text{II}}(\text{Cl}_2\text{bdt})_2]$ ; see the Experimental Section for further details and Table 1 for select bond lengths. One equivalent of butyronitrile is also present in the crystal but is omitted here for clarity, just as the hydrogen atoms.

The electronic structure of this Co(II) species was further studied by EPR spectroscopy. Unlike the  $S_t = 1$  Co(III) species, which is EPR silent, the reduced Co(II) complex has a non-integer spin ground state and gives an EPR signal. As expected, due to the  $I = 7/2$  nuclear spin of Co, the EPR spectrum shows Co hyperfine, see Figure 3. The EPR spectrum

is fit as a Co(II)  $S_t = 1/2$  species, with high  $A$  values and  $g$  strain as is evident from the relatively smooth appearance of the EPR spectrum. The  $g_z$  value is found to be  $g_z = 2.95$  while  $g_x$  and  $g_y$  are near  $g = 2$ , corresponding to a highly axial species. The exact fitting parameters used here are given in the caption of Figure 3.

**Table 1.** Comparison of average bond lengths between the Co(III) and Co(II) states of  $\text{Co}(\text{Cl}_2\text{bdt})_2$ . The bond lengths for the Co(III) complex are taken from Ref. [2].

Bond	Co(II) Catalyst (Å)	Co(III) Catalyst (Å)
Co-S	2.182 (4)	2.164 (5)
S-C	1.749 (7)	1.750 (3)
C-C	1.395 (14)	1.393 (11)

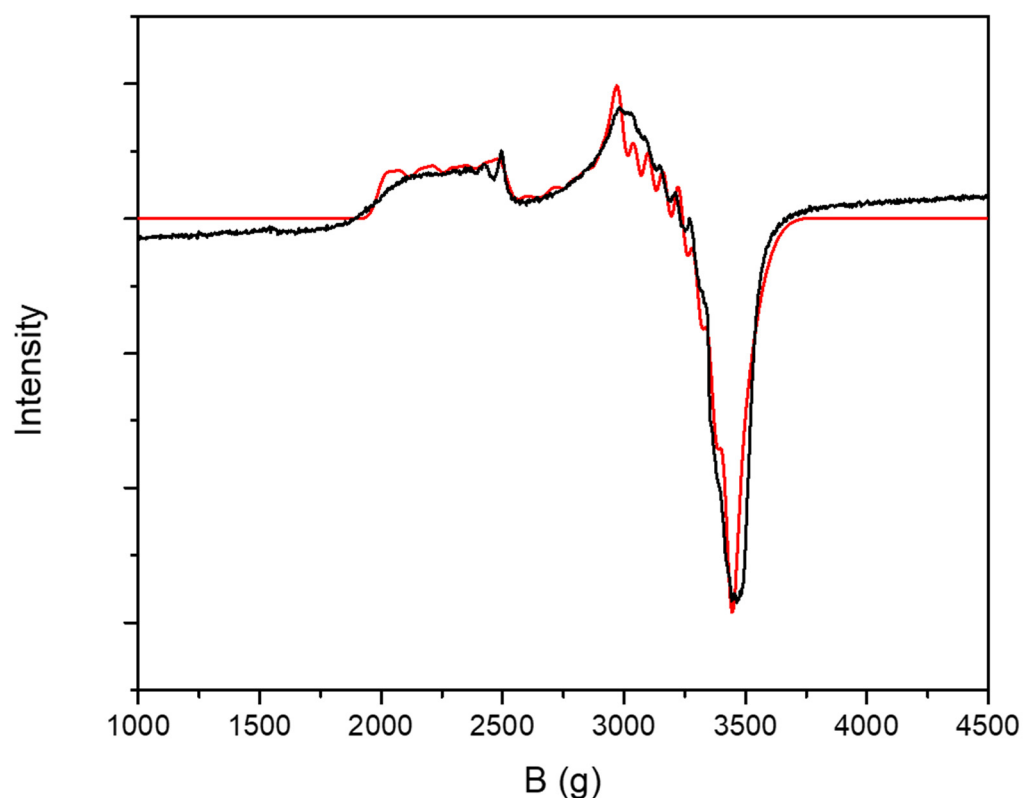


**Figure 3.** EPR spectrum of  $[\text{TBA}][\text{CoCp}_2][\text{Co}^{\text{II}}(\text{Cl}_2\text{bdt})_2]$ , 1 mM in THF, measured at 10 K. The experimental spectrum is given in black, and the fit is shown in red. The fit parameters are  $g = 1.95, 2.07, 2.95$ ;  $g_{\text{strain}} = 0.06, 0.014, 0.04$ ;  $A(\text{Co}) = \text{not fit}, 180, 280 \text{ MHz}$ .

Further, the Co(III) and Co(II) complexes were studied by MCD spectroscopy. Both species show temperature-sensitive C-term signals, as expected for paramagnetic complexes, as shown in Figure 4. Interestingly, the Co(III) species only shows mild temperature dependence until higher temperatures are reached, see the decrease in intensity at 20 and 50 K. This indicates strong axial zero-field splitting for the complex, with a negative  $D$  value. The shape of the bands for the complex  $[\text{Co}^{\text{III}}(\text{Cl}_2\text{bdt})_2]^{2-}$  aligns well with previously reported MCD data for the complex  $[\text{TBA}][\text{Co}^{\text{III}}(\text{tb-bdt})_2]$ , see Ref. [16] for further discussion. This supports similar electronic structures for the two species, and similar assignments of the optical spectra, featuring several strong ligand-to-metal charge-transfer (LMCT) excitations in the visible region, and a few weaker, symmetry-forbidden d-d transitions [16]. Due to this similarity and the fact that the Co(III) complexes are well studied [14], the electronic structure of this oxidation state was not further explored.

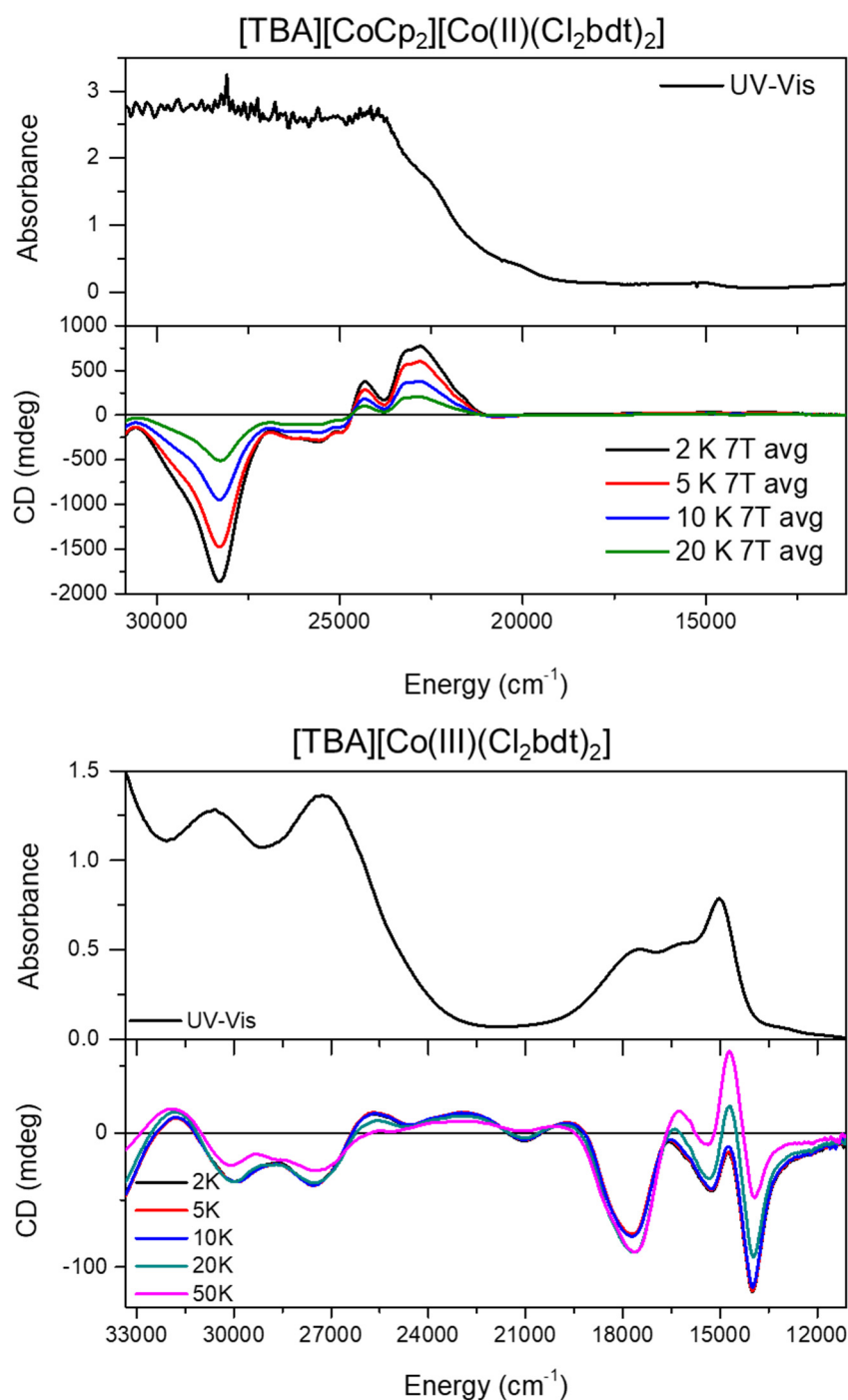


**Figure 4.** Comparison of the UV-Vis and MCD spectra of  $[Co^{II}(Cl_2bdt)_2]^{2-}$  (top) to those of  $[Co^{III}(Cl_2bdt)_2]^-$  (bottom). Co(II) MCD samples were prepared in butyronitrile at 0.5 mM, and a standard run was conducted at  $\pm 7$ ,  $\pm 5$ ,  $\pm 3$ ,  $\pm 1$ , and 0 T, and 2, 5, 10, and 20 K. Shown here are the 7T data for each temperature. The UV-Vis spectrum shown is that of  $[TBA][CoCp_2][Co^{II}(Cl_2bdt)_2]$  at 0.5 mM in butyronitrile, using the same sample that was used to obtain the MCD data. The Co(III) data were measured on a polystyrene film sample. A standard run was conducted with 50 K data also included. Shown here are the 7T data for each temperature. The UV-Vis spectrum is that of  $[TBA][Co^{III}(Cl_2bdt)_2]$ , 0.1 mM in acetonitrile. Data for the Co(III) complex were also obtained in butyronitrile at 0.5 mM (not shown). For each complex, only MCD data where the voltage curve is below 750 V are shown.

The MCD spectra of the Co(II) complex match well with the UV-Vis data of this species (see Figure 4), showing features at high energy, but much less intensity in the visible region. The spectra are highly temperature dependent, similarly showing C-term behavior consistent with a paramagnetic complex. The saturation curves of this species were determined for the two most intense bands, at 439 nm ( $22,779\text{ cm}^{-1}$ ) and 353 nm ( $28,328\text{ cm}^{-1}$ ), as shown in Figure 5. These saturation curves overlay neatly, which is consistent with a  $S_t = 1/2$  species, as further suggested by the square-planar geometry and indicated by the EPR fit. These saturation curves can indeed be fit as a  $S_t = 1/2$  species, using the  $g$  values obtained from the EPR fit.

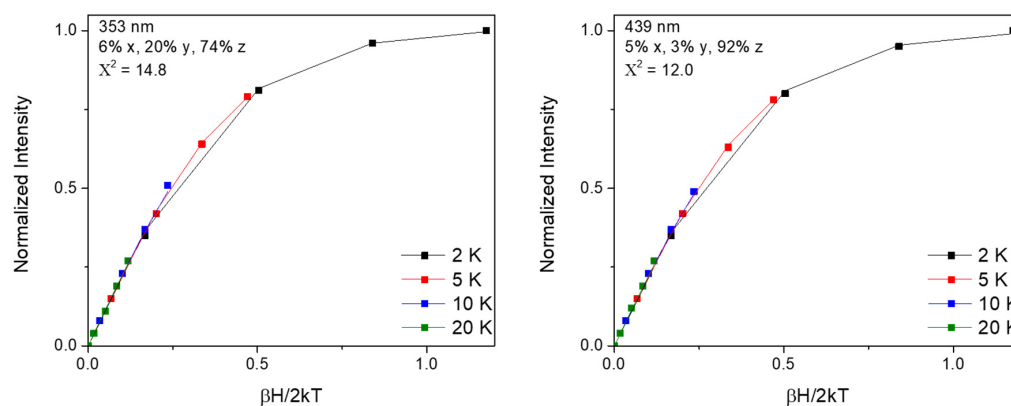


**Figure 5.** Saturation behavior of the two main bands of  $[\text{Co}^{\text{II}}(\text{Cl}_2\text{bdt})_2]^{2-}$ . **Left:** the saturation behavior of the positive band at 439 nm ( $22,779\text{ cm}^{-1}$ ). **Right:** the saturation behavior of the negative band at 353 nm ( $28,328\text{ cm}^{-1}$ ). Experimental data points are shown with color-coded squares. Fits of the VTVH MCD data are shown with color-coded lines. The fit with  $S_t = 1/2$  and the resulting polarizations are shown in the panels (but note that the polarizations are generally not well defined for  $S_t = 1/2$  systems). The lack of nesting of the saturation curves together with the excellent agreement of the fits with experiment provides strong evidence that the complex has a  $S_t = 1/2$  ground state, as further supported by the EPR data.

### 3. Materials and Methods

#### 3.1. General Synthesis and Chemicals

Chemicals were used as received except for cobaltocene, which was sublimed before use for purification. To maintain an air-free atmosphere required for the experiments, a nitrogen glovebox or Schlenk line was employed. Specifically for the handling of  $[\text{Co}(\text{Cl}_2\text{bdt})_2]^{2-}$ , Schlenk line techniques using Ar as an inert gas were employed.  $[\text{TBA}][\text{Co}(\text{Cl}_2\text{bdt})_2]$  was synthesized according to the reported methods [5,15].

#### 3.2. Reduction Procedures

To obtain  $[\text{TBA}][\text{CoCp}_2][\text{Co}(\text{II})(\text{Cl}_2\text{bdt})_2]$  via chemical reduction, one equivalent of  $\text{CoCp}_2$  was added to a solution of  $[\text{TBA}][\text{Co}(\text{Cl}_2\text{bdt})_2]$  in the desired solvent. For example, for EPR sample preparation, a 2 mM solution of  $[\text{TBA}][\text{Co}(\text{Cl}_2\text{bdt})_2]$  in THF was prepared. Then, to 0.75 mL of this deep blue solution, 0.2 mL 7.5 mM cobaltocene solution in THF was added. Upon the addition of the cobaltocene solution, the color changed to a clear yellow. This solution was then diluted to 1.5 mL to yield a 1 mM solution of  $[\text{TBA}][\text{CoCp}_2][\text{Co}(\text{II})(\text{Cl}_2\text{bdt})_2]$ .

For electrochemical reduction, a solution of 0.5–3 mM  $[\text{TBA}][\text{Co}(\text{Cl}_2\text{bdt})_2]$  in 0.1 M  $[\text{TBA}](\text{PF}_6)$  in acetonitrile or acetone was reduced at  $-0.2\text{ V}$  more negative than the  $\text{Co}(\text{III}/\text{II})$  redox couple, until the current dropped and the change in color from blue to yellow was complete; see Figure S2 for a representative example. A two-part electrochemical cell with excess ferrocene (Fc) as a sacrificial oxidant in the counter electrode half-cell was employed. The charge passed may be slightly more than necessary for the reduction of  $[\text{TBA}][\text{Co}(\text{Cl}_2\text{bdt})_2]$ , depending on the degree of anaerobicity of the electro-

chemical cell. The reference was an Ag wire pseudo-reference electrode; however, the data were not referenced to  $\text{Fc}^+/\text{Fc}$  after electrolysis to maintain the purity of the Co(II) solution.

### 3.3. Instrumentation

UV-Vis spectra were obtained on an Analytical Jena Specord S600 instrument. The MCD spectroscopy setup consists of an Oxford SM4000 cryostat and a JASCO J-815 CD spectrometer. The SM4000 cryostat uses a liquid helium-cooled super-conducting magnet, providing magnetic fields of 0–7 T. The light source for the JASCO J-815 CD spectrometer is a gaseous nitrogen-cooled xenon lamp, and the detector is a photomultiplier in the UV-Vis range. The samples are loaded into the Oxford Cryostat variable temperature insert (VTI) chamber, which can reach temperatures of 1.5–300 K and has four optical windows made of Suprasil B quartz for optical access to the sample. Here, temperatures of 2, 5, 10, 20 K, and for  $[\text{TBA}][\text{Co}(\text{Cl}_2\text{bdt})_2]$ , 50 K were used for the MCD measurements, and spectra were obtained at  $\pm 7$ ,  $\pm 5$ ,  $\pm 3$ ,  $\pm 1$ , and 0 T at each temperature. The EPR measurements were conducted on a Bruker X-band EMX spectrometer, which is equipped with an Oxford liquid helium cryostat. The EPR data were fit using the program SpinCount (Prof. M. P. Hendrich at Carnegie Mellon University) [26]. Electrochemical measurements were conducted using a CH Instruments (Austin, TX, USA) CHI600E potentiostat.

### 3.4. X-ray Crystallography

Green plates of  $(\text{CoCp}_2)_2[\text{Co}^{\text{II}}(\text{Cl}_2\text{bdt})_2]$  were grown from the slow evaporation of a 0.5 mM butyronitrile solution of the compound at  $-20^\circ\text{C}$  over the course of a month. A crystal of dimensions  $0.10 \times 0.08 \times 0.04$  mm was mounted on a Rigaku AFC10K Saturn 944+ CCD-based X-ray diffractometer equipped with a low-temperature device and a Micromax-007HF Cu-target micro-focus rotating anode ( $\lambda = 1.54187 \text{ \AA}$ ) operated at 1.2 kW power (40 kV, 30 mA). The X-ray intensities were measured at 85(1) K with the detector placed at a distance of 42.00 mm from the crystal. A total of 2028 images were collected with an oscillation width of  $1.0^\circ$  in  $\omega$ . The exposure times were 1 s. for the low-angle images, and 5 s for high angle. Rigaku d\*trek images were exported to CrysAlisPro for processing and corrected for absorption. The integration of the data yielded a total of 55,226 reflections to a maximum  $2\theta$  value of  $138.85^\circ$  of which 12,797 were independent and 11,576 were greater than  $2\sigma(I)$ . The final cell constants (Table S1) were based on the xyz centroids of 15,456 reflections above  $10\sigma(I)$ . Analysis of the data showed negligible decay during data collection. The structure was solved and refined with the Bruker SHELXTL (version 2018/3) software package, using the space group  $P2(1)$  with  $Z = 4$  for the formula  $\text{C}_{36}\text{H}_{31}\text{NCl}_4\text{S}_2\text{Co}_3$ . All non-hydrogen atoms were refined anisotropically with the hydrogen atoms placed in idealized positions. Full matrix least-squares refinement based on  $F^2$  converged at  $R1 = 0.0642$  and  $wR2 = 0.1634$  [based on  $I > 2\sigma(I)$ ],  $R1 = 0.0708$  and  $wR2 = 0.1712$  for all data. Additional details are presented in Tables S1–S6 and the CIF file deposited at the CCDC, CCDC number: 2309250.

## 4. Conclusions

In summary, the complex  $[\text{TBA}][\text{Co}^{\text{III}}(\text{Cl}_2\text{bdt})_2]$  has been reduced to the Co(II) form electrochemically and chemically. This mimics the first step in electrocatalysis, reduction, for this set of HER catalysts. The oxygen-sensitive Co(II) complex was characterized by X-ray crystallography, UV-Vis, EPR, and MCD spectroscopy. From these characterization techniques, the Co(II) species has been shown to have a square-planar structure, with a metal-centered reduction and a  $S_t = 1/2$  ground state. This is in contrast to the DFT-predicted, tetrahedral Co(II) geometry for this species [18]. These results show that, unlike previously predicted, dephysisorption upon a structural distortion of  $\text{Co}^{\text{III}}(\text{bdt})_2$  complexes upon reduction to the Co(II) state is not a primary mode of deactivation of these catalysts when physisorbed to graphitic surfaces for the purpose of HER. Further, our results question the next steps of the predicted HER mechanism (Scheme 1), as the related Co bis(diaryldithiolene) type complexes are predicted to protonate at their Co center atoms

when square planar, rather than on the sulfur atoms [19,21]. Additionally, a study on an HER active 2D MOF with square-planar Co bis(benzenedithiolate) active sites reported that only Co sites, not S, were active in the HER mechanism [27]. This suggests that, now that the Co(II) state of HER active Co bis(benzenedithiolate) type complexes is known to be a doublet square-planar species, protonation may be expected to occur at the Co center, rather than the sulfur atoms as previously calculated. Research on characterizing the reactivity of  $[\text{Co}^{\text{II}}(\text{Cl}_2\text{bdt})_2]^{2-}$  and on isolating the next intermediates in the HER cycle is underway in our group.

**Supplementary Materials:** The Supporting Information is available free of charge at <https://www.mdpi.com/article/10.3390/inorganics12030075/s1> and contains further spectroscopic data and tables of the X-ray crystallographic parameters. Figure S1: Comparison of the UV-Vis spectra of the product of Co(II) oxidation by ambient air and the authentic  $[\text{Co}^{\text{III}}(\text{Cl}_2\text{bdt})_2]^-$  starting complex; Figure S2: Electrochemical reduction of  $[\text{TBA}][\text{Co}^{\text{III}}(\text{Cl}_2\text{bdt})_2]$  to  $[\text{TBA}]_2[\text{Co}^{\text{II}}(\text{Cl}_2\text{bdt})_2]$ ; Figure S3: UV-Vis spectrum of electrochemically-reduced  $[\text{TBA}]_2[\text{Co}^{\text{II}}(\text{Cl}_2\text{bdt})_2]$ , 0.1 mM in MeCN; Table S1: Crystal data and structure refinement for  $[\text{CoCp}_2]_2[\text{Co}^{\text{II}}(\text{Cl}_2\text{bdt})_2]$ ; Table S2: Atomic coordinates and equivalent isotropic displacement parameters for  $[\text{CoCp}_2]_2[\text{Co}^{\text{II}}(\text{bdt})_2]$ ; Table S3: Bond lengths and angles for  $[\text{CoCp}_2]_2[\text{Co}^{\text{II}}(\text{bdt})_2]$ ; Table S4: Anisotropic displacement parameters for  $[\text{CoCp}_2]_2[\text{Co}^{\text{II}}(\text{bdt})_2]$ ; Table S5: Hydrogen coordinates and isotropic displacement parameters for  $[\text{CoCp}_2]_2[\text{Co}^{\text{II}}(\text{bdt})_2]$ ; Table S6: Torsion angles for  $[\text{CoCp}_2]_2[\text{Co}^{\text{II}}(\text{bdt})_2]$ .

**Author Contributions:** Conceptualization, V.A.L. and N.L.; Methodology, V.A.L. and N.L.; Formal Analysis, V.A.L.; Investigation, V.A.L. and J.W.K. (V.A.L. performed the experiments described here, except for the X-ray crystallography, which was performed by J.W.K., who acquired the data and solved the structure.); Resources, N.L.; Writing—Original Draft Preparation, V.A.L.; Writing—Review and Editing, N.L. and V.A.L.; Visualization, V.A.L. and J.W.K.; Supervision, N.L.; Project Administration, N.L.; Funding Acquisition, N.L. and V.A.L. All authors have read and agreed to the published version of the manuscript.

**Funding:** VAL acknowledges support from a University of Michigan Rackham Predoctoral Fellowship. Acknowledgment is made for funding from NSF grant CHE-0840456 for X-ray instrumentation.

**Data Availability Statement:** The data presented in this study are available on request from the corresponding author. X-ray crystallographic data are available free of charge from the Cambridge Crystallographic Data Centre (CCDC) under deposition no. 2309250.

**Conflicts of Interest:** The authors declare no conflicts of interest.

## References

1. McNamara, W.R.; Han, Z.; Alperin, P.J.; Brennessel, W.W.; Holland, P.L.; Eisenberg, R. A Cobalt–Dithiolene Complex for the Photocatalytic and Electrocatalytic Reduction of Protons. *J. Am. Chem. Soc.* **2011**, *133*, 15368–15371. [[CrossRef](#)] [[PubMed](#)]
2. McNamara, W.R.; Han, Z.; Yin, C.-J.M.; Brennessel, W.W.; Holland, P.L.; Eisenberg, R.; By, E.; Meyer, T.J. Cobalt–Dithiolene Complexes for the Photocatalytic and Electrocatalytic Reduction of Protons in Aqueous Solutions. *Proc. Natl. Acad. Sci. USA* **2012**, *109*, 15594–15599. [[CrossRef](#)] [[PubMed](#)]
3. Eady, S.C.; Peczonczyk, S.L.; Maldonado, S.; Lehnert, N. Facile Heterogenization of a Cobalt Catalyst via Graphene Adsorption: Robust and Versatile Dihydrogen Production Systems. *Chem. Commun.* **2014**, *50*, 8065–8068. [[CrossRef](#)] [[PubMed](#)]
4. Eady, S.C.; MacInnes, M.M.; Lehnert, N. A Smorgasbord of Carbon: Electrochemical Analysis of Cobalt–Bis(Benzenedithiolate) Complex Adsorption and Electrocatalytic Activity on Diverse Graphitic Supports. *ACS Appl. Mater. Interfaces* **2016**, *8*, 23624–23634. [[CrossRef](#)] [[PubMed](#)]
5. Eady, S.C.; MacInnes, M.M.; Lehnert, N. Immobilized Cobalt Bis(Benzenedithiolate) Complexes: Exceptionally Active Heterogeneous Electrocatalysts for Dihydrogen Production from Mildly Acidic Aqueous Solutions. *Inorg. Chem.* **2017**, *56*, 11654–11667. [[CrossRef](#)]
6. Downes, C.A.; Marinescu, S.C. Efficient Electrochemical and Photoelectrochemical H<sub>2</sub> Production from Water by a Cobalt Dithiolene One-Dimensional Metal–Organic Surface. *J. Am. Chem. Soc.* **2015**, *137*, 13740–13743. [[CrossRef](#)] [[PubMed](#)]
7. Clough, A.J.; Yoo, J.W.; Mecklenburg, M.H.; Marinescu, S.C. Two-Dimensional Metal–Organic Surfaces for Efficient Hydrogen Evolution from Water. *J. Am. Chem. Soc.* **2015**, *137*, 118–121. [[CrossRef](#)]
8. Downes, C.A.; Clough, A.J.; Chen, K.; Yoo, J.W.; Marinescu, S.C. Evaluation of the H<sub>2</sub> Evolving Activity of Benzenehexathiolate Coordination Frameworks and the Effect of Film Thickness on H<sub>2</sub> Production. *ACS Appl. Mater. Interfaces* **2018**, *10*, 1719–1727. [[CrossRef](#)]

9. Downes, C.A.; Marinescu, S.C. Understanding Variability in the Hydrogen Evolution Activity of a Cobalt Anthracenetetrathiolate Coordination Polymer. *ACS Catal.* **2017**, *7*, 8605–8612. [[CrossRef](#)]
10. Larson, V.A.; Lehnert, N. Covalent Attachment of Cobalt Bis(Benzylaminedithiolate) to Reduced Graphene Oxide as a Thin Film Electrocatalyst for Hydrogen Production with Remarkable Dioxygen Tolerance. *ACS Catal.* **2024**, *14*, 192–210. [[CrossRef](#)]
11. Dalle, K.E.; Warnan, J.; Leung, J.J.; Reuillard, B.; Karmel, I.S.; Reisner, E. Electro- and Solar-Driven Fuel Synthesis with First Row Transition Metal Complexes. *Chem. Rev.* **2019**, *119*, 2752–2875. [[CrossRef](#)] [[PubMed](#)]
12. Drosou, M.; Kamatsos, F.; Mitsopoulou, C.A. Recent Advances in the Mechanisms of the Hydrogen Evolution Reaction by Non-Innocent Sulfur-Coordinating Metal Complexes. *Inorg. Chem. Front.* **2019**, *7*, 37–71. [[CrossRef](#)]
13. Gray, H.B.; Billig, E. The Electronic Structures of Square-Planar Metal Complexes. III. High-Spin Planar Cobalt(I) and Iron(I). *J. Am. Chem. Soc.* **1963**, *85*, 2019–2020. [[CrossRef](#)]
14. Eisenberg, R.; Gray, H.B. Noninnocence in Metal Complexes: A Dithiolene Dawn. *Inorg. Chem.* **2011**, *50*, 9741–9751. [[CrossRef](#)] [[PubMed](#)]
15. Baker-Hawkes, M.J.; Billig, E.; Gray, H.B. Characterization and Electronic Structures of Metal Complexes Containing Benzene-1,2-Dithiolate and Related Ligands. *J. Am. Chem. Soc.* **1966**, *88*, 4870–4875. [[CrossRef](#)]
16. Ray, K.; Begum, A.; Weyhermüller, T.; Piligkos, S.; Van Slageren, J.; Neese, F.; Wieghardt, K. The Electronic Structure of the Isoelectronic, Square-Planar Complexes  $[\text{Fe}^{\text{II}}(\text{L})_2]^{2-}$  and  $[\text{Co}^{\text{III}}(\text{L}^{\text{Bu}})_2]^-$  ( $\text{L}^{2-}$  and  $(\text{L}^{\text{Bu}})^{2-}$  = Benzene-1,2-Dithiolates): An Experimental and Density Functional Theoretical Study. *J. Am. Chem. Soc.* **2005**, *127*, 4403–4415. [[CrossRef](#)]
17. Benedito, F.L.; Petrenko, T.; Bill, E.; Weyhermüller, T.; Wieghardt, K. Square Planar Bis(3,6-Bis(Trimethylsilyl)Benzene-1,2-Dithiolato)metal Complexes of CrII, CoIII, and RhII: An Experimental and Density Functional Theoretical Study. *Inorg. Chem.* **2009**, *48*, 10913–10925. [[CrossRef](#)]
18. Solis, B.H.; Hammes-Schiffer, S. Computational Study of Anomalous Reduction Potentials for Hydrogen Evolution Catalyzed by Cobalt Dithiolene Complexes. *J. Am. Chem. Soc.* **2012**, *134*, 15253–15256. [[CrossRef](#)]
19. Letko, C.S.; Panetier, J.A.; Head-Gordon, M.; Tilley, T.D. Mechanism of the Electrocatalytic Reduction of Protons with Diaryldithiolene Cobalt Complexes. *J. Am. Chem. Soc.* **2014**, *136*, 9364–9376. [[CrossRef](#)]
20. Zhang, C.; Prignot, E.; Jeannin, O.; Vacher, A.; Dragoë, D.; Camerel, F.; Halime, Z.; Gramage-Doria, R. Efficient Hydrogen Production at PH 7 in Water with a Heterogeneous Electrocatalyst Based on a Neutral Dimeric Cobalt-Dithiolene Complex. *ACS Catal.* **2023**, *13*, 2367–2373. [[CrossRef](#)]
21. Panetier, J.A.; Letko, C.S.; Tilley, T.D.; Head-Gordon, M. Computational Characterization of Redox Non-Innocence in Cobalt-Bis (Diaryldithiolene)-Catalyzed Proton Reduction. *J. Chem. Theory Comput.* **2016**, *12*, 223–230. [[CrossRef](#)] [[PubMed](#)]
22. Sawyer, D.T.; Srivatsa, G.S.; Bodini, M.E.; Schaefer, W.P.; Wing, R.M. Redox Chemistry and Spectroscopy of Toluene-3, 4-Dithiol (TDTH2) and of Its M (TDT) 22-/-Complexes with Zinc (II), Copper (II), Nickel (II), Cobalt (II), Iron (II), and Manganese (II). Formation of a Stable Dn-(Cn) Bond upon Oxidation by One Ele. *J. Am. Chem. Soc.* **1986**, *108*, 936–942. [[CrossRef](#)]
23. Ray, K. Do S, S'-Coordinated o-Dithiobenzosemiquinonate(1-) Radicals Exist in Coordination Compounds? A Combined Experimental and Computational Study. Ph.D. Thesis, Ruhr-Universität Bochum, Bochum, Germany, 2005.
24. Cerdeira, A.C.; Afonso, M.L.; Santos, I.C.; Pereira, L.C.J.; Coutinho, J.T.; Rabaça, S.; Simão, D.; Henriques, R.T.; Almeida, M. Synthesis, Structure and Physical Properties of Transition Metal Bis 4-Cyanobenzene-1,2-Dithiolate Complexes  $[\text{M}(\text{Cbdt})_2]^{Z-}$  (M = Zn, Co, Cu, Au, Ni, Pd, Z = 0, 1, 2). *Polyhedron* **2012**, *44*, 228–237. [[CrossRef](#)]
25. Yang, L.; Powell, D.R.; Houser, R.P. Structural Variation in Copper (I) Complexes with Pyridylmethylamide Ligands: Structural Analysis with a New Four-Coordinate Geometry Index,  $\tau_4$ . *Dalt. Trans.* **2007**, 955–964. [[CrossRef](#)]
26. Petasis, D.T.; Hendrich, M.P. Quantitative Interpretation of Multifrequency Multimode EPR Spectra of Metal Containing Proteins, Enzymes, and Biomimetic Complexes. *Methods Enzymol.* **2015**, *563*, 171–208. [[CrossRef](#)]
27. Chen, K.; Downes, C.A.; Schneider, E.; Goodpaster, J.D.; Marinescu, S.C. Improving and Understanding the Hydrogen Evolving Activity of a Cobalt Dithiolene Metal–Organic Framework. *ACS Appl. Mater. Interfaces* **2021**, *13*, 16384–16395. [[CrossRef](#)]

**Disclaimer/Publisher’s Note:** The statements, opinions and data contained in all publications are solely those of the individual author(s) and contributor(s) and not of MDPI and/or the editor(s). MDPI and/or the editor(s) disclaim responsibility for any injury to people or property resulting from any ideas, methods, instructions or products referred to in the content.